

Article

State of Health Estimation of Li-Ion Battery via Incremental Capacity Analysis and Internal Resistance Identification Based on Kolmogorov–Arnold Networks

Jun Peng ¹, Xuan Zhao ^{1,*}, Jian Ma ¹, Dean Meng ¹, Shuhai Jia ², Kai Zhang ¹, Chenyan Gu ¹ and Wenhao Ding ¹

¹ School of Automobile, Chang'an University, Xi'an 710064, China; pengjun@chd.edu.cn (J.P.)

² School of Mechanical Engineering, Xi'an Jiaotong University, Xi'an 710049, China

* Correspondence: zhaoxuan@chd.edu.cn

Abstract: An accurate estimation of the state of health (SOH) of Li-ion batteries is critical for the efficient and safe operation of battery-powered systems. Traditional methods for SOH estimation, such as Coulomb counting, often struggle with sensitivity to measurement noise and time-consuming tests. This study addresses this issue by combining incremental capacity (IC) analysis and a novel neural network, Kolmogorov–Arnold Networks (KANs). Fifteen features were extracted from IC curves and a 2RC equivalent circuit model was used to identify the internal resistance of batteries. Recursive least squares were used to identify the parameters of the equivalent circuit model. IC features and internal resistance were considered as input variables to establish the SOH estimation model. Three commonly used machine learning methods (BP, LSTM, TCN) and two hybrid algorithms (LSTM-KAN and TCN-KAN) were used to establish the SOH estimation model. The performance of the five models was compared and analyzed. The results demonstrated that the hybrid models integrated with the KAN performed better than the conventional models, and the LSTM-KAN model had higher estimation accuracy than that of the other models. The model achieved a mean absolute error of less than 0.412% in SOH prediction in the test and validation dataset. The proposed model does not require complete charge and discharge data, which provides a promising tool for the accurate monitoring and fast detection of battery SOH.

Keywords: SOH estimation; KAN; incremental capacity analysis; internal resistance; Li-ion battery



Citation: Peng, J.; Zhao, X.; Ma, J.; Meng, D.; Jia, S.; Zhang, K.; Gu, C.; Ding, W. State of Health Estimation of Li-Ion Battery via Incremental Capacity Analysis and Internal Resistance Identification Based on Kolmogorov–Arnold Networks. *Batteries* **2024**, *10*, 315. <https://doi.org/10.3390/batteries10090315>

Academic Editors: Remus Teodorescu and Xin Sui

Received: 16 July 2024

Revised: 30 August 2024

Accepted: 2 September 2024

Published: 4 September 2024



Copyright: © 2024 by the authors. Licensee MDPI, Basel, Switzerland. This article is an open access article distributed under the terms and conditions of the Creative Commons Attribution (CC BY) license (<https://creativecommons.org/licenses/by/4.0/>).

1. Introduction

Electric and hybrid vehicles have experienced rapid growth in recent years. Lithium-ion (Li-ion) batteries are a critical component of electric vehicles (EVs) in providing power for vehicles. The application scale of Li-ion batteries in EVs is far larger than other types of batteries owing to several advantages of Li-ion batteries, including high energy density, a long lifespan, low maintenance requirements, etc. [1]. A battery management system (BMS) plays a key role in ensuring the safe and efficient operation of a vehicle's battery system. State of health (SOH) estimation is an indispensable function for the BMS, which contributes to determining retained capacity and remaining useful life, optimizing the charging/discharging process to extend the life and prevent the premature failure of batteries [2].

While the SOH is crucial for a battery management system (BMS) to function effectively, an accurate definition and calculation method for the SOH has not been universally established [3]. Generally, capacity fading and the increase in internal resistance are commonly used indicators to assess the SOH of a battery. To obtain variation in capacity and resistance, the most commonly used approaches are to measure the current and voltage parameters of a battery to derive the two indicators. The approaches to acquiring the SOH from the current and voltage data can be categorized into two types: direct computation [4] or model-based machine learning [5]. The former method includes coulomb counting,

internal resistance/impedance calculation, etc. The method based on machine learning uses the current/voltage data or other variables derived from them to establish a neural network model to predict the change in capacity and impedance.

Coulomb counting is an integral of current over time that uses a current sensor to monitor the current during the charge/discharge process, and the maximum increased/elapsed capacity can be calculated. The SOH of batteries can be determined through the ratio of maximum capacity to the rated capacity [6]. Battery SOH can also be defined from the perspective of internal resistance evolution. The internal resistance increases with the degeneration of cells. The difference between the internal resistance at the end of battery life and the fresh stage is regarded as a basis for evaluating the SOH [7]. This resistance, R , can be obtained by Ohm's law or parameter identification based on an equivalent circuit model.

These above approaches have their limitations. For instance, the Coulomb counting method is only available in a full charge/discharge process to obtain the current maximum capacity. The accuracy of resistance measurement is influenced by the battery state of charge and the environmental temperature. Therefore, the SOH estimation method based on the calculation of capacity and resistance is restricted by the working circumstance of batteries and has low efficiency and poor scalability. To overcome this challenge, data-driven approaches are proposed to predict the SOH based on the history data of the current, voltage, capacity, etc., wherein the statistical analysis method and machine learning are mostly used in the establishment of SOH estimation models, such as gray relation analysis [8], support vector regression (SVR) [9], XGboost [10], back propagation (BP) neural network [11,12], and Long Short-Term Memory (LSTM) network [13,14]. In May 2024, a team of researchers at the Massachusetts Institute of Technology introduced the Kolmogorov–Arnold Network (KAN), a novel neural network architecture differing from the multilayer perceptron (MLP) network [15]. This innovative approach is grounded in the theoretical principles of the Kolmogorov–Arnold representation theorem, which offers a powerful framework for decomposing complex multivariate functions into simpler, univariate components [16].

The key steps of data-driven approaches are defining effective informative inputs and establishing a robust estimation model. Commonly, the current, voltage, and temperature data in the charge/discharge process are set as the inputs. Compared to the unprocessed current and voltage data, the features derived from them can better describe the battery aging mechanism and understand the materials' properties, interfacial phenomena, and electrochemical behavior inside cells, such as electrochemical impedance spectroscopy (EIS), incremental capacity (IC), and differential voltage (DV). Incremental capacity analysis is a widely used approach to identify and quantify the changes in electrochemical reactions inside a battery [17–19]. It is assumed that the cell is at an equilibrium state during a charge/discharge process with an extremely low current rate (C-rate). However, the low C-rate charge/discharge process cannot be performed in field application due to the high cost of time. For SOH estimation, it is unnecessary to pay more attention to the details of the battery degradation process; rather, it is necessary to just focus on the remaining battery capacity at a certain moment. Therefore, a pragmatic solution is proposed to replace a low C-rate with a large C-rate. Therefore, there is increasing research on using IC curve data for SOH prediction. Li et al. adopted the Gaussian filter to process IC curves and use the position and height of the curve peak as the feature of interest for the SOH estimation of a high-energy NMC li-ion battery [20]. In ref. [21], IC curves were used to estimate battery SOH based on SVR. Beltran et al. investigated the performance of different machine learning methods in the estimation of retained capacity, using IC curves [22].

The internal resistance of a battery comprises several components that collectively determine how much opposition the battery presents to the flow of the electric current. These components can be broadly categorized into three main types: ohmic resistance, polarization internal resistance, and electrochemical impedance [23]. Ohmic resistance is the straightforward electrical resistance of the battery's conductive materials (electrodes, electrolytes, and connectors) [24]. Electrochemical impedance is more complex and includes

various factors associated with the battery's electrochemical processes, including charge transfer resistance, and solid electrolyte interphase (SEI) resistance [25]. As a battery undergoes repeated charge and discharge cycles, various degradation will occur, such as the growth of the SEI layer, electrolyte decomposition, and loss of active material. These processes lead to an increase in the internal resistance of the battery. An increase in internal resistance is a key indicator of these degradation processes [26,27]. It reflects the battery's reduced efficiency in conducting current, which is directly related to its aging and SOH. Internal resistance is a valuable and reliable indicator for estimating the SOH of a battery [28].

In the above works, only IC curve features were used as input parameters for modeling. IC curve features are susceptible to the environmental temperature and current rate. In this work, we employed both internal resistance parameters and IC features as inputs to establish a hybrid model. Moreover, the aforementioned machine learning models were based on MLP. KANs, as an emerging network structure, have the potential to become an alternative to MLP. Therefore, we proposed an SOH estimation approach by the combination of features extracted from IC curves and internal resistance based on the KAN algorithm. First, an accelerated aging test was performed to prepare the degradation data. Next, the raw data of charge cycles were processed to obtain the IC curves, and some advanced filter algorithms were adopted to smooth the original IC curves. The peaks of IC curves often correspond to phase transitions within the battery's active materials. For example, in lithium-ion batteries, lithium intercalates into or de-intercalates from electrode materials. In some cases, an IC curve peak might indicate lithium plating, which is a form of battery degradation [29,30]. The dips represent gaps between different intercalation stages within the battery's active materials. The peaks and dips of an IC curve of a battery provide important insights into the battery's state and characteristics. Therefore, the features of IC curves were extracted as the inputs of SOH estimation models, including the height, width, and position of peaks and dips. Then, a 2RC equivalent circuit model and the recursive least squares (RLS) algorithm were used to identify the internal resistance of batteries. Three commonly used machine learning methods were used to establish the SOH estimation model, including BP, LSTM, and Temporal Convolutional Networks (TCNs), and the KAN was adopted to build hybrid models (LSTM-KAN and TCN-KAN) for SOH estimation. Furthermore, we compared the estimation performance of five models and investigated the effect of adding the KAN on the original model performance. The model with the best performance among the five was chosen to evaluate the accuracy of the SOH estimation model with different input variables. To our best knowledge, this was the first time the KAN was used to estimate the SOH of Li-ion batteries.

The rest of this paper is organized as follows. In Section 2, we describe the experiment and data preparation in detail, including the battery aging test conditions, the feature extraction from the IC curve, and internal resistance identification. The principle of LSTM-KAN and the SOH estimation model framework based on LSTM-KAN are shown in Section 3. The prediction results of the proposed SOH estimation model and the comparison between different models and input parameters are shown in Section 4, and the conclusions are drawn in Section 5.

2. Experiment and Data Preparation

2.1. Battery Aging Test

To obtain the aging data of batteries, a test platform was established, as shown in Figure 1. A battery testing system, BTS4000 (Neware, Shenzhen, China), was used to run the defined charge/discharge cycles. Eight commercial LiFePO₄ batteries were tested in the experiment, and cell specification is shown in Table 1. The cells were placed in the temperature control chamber to maintain a stable ambient temperature during the charging/discharging process. Capacity degeneration is closely related to the charging environmental temperature. To accelerate the aging process, the ambient temperature for charging and discharging was set at 35 °C. A standard charge/discharge regime was

applied on the cells, which was composed of constant current (CC) charging with 1C to the cut-off voltage, then constant voltage charging to the cut-off current of C/20, and CC discharging with 1C to a cut-off voltage. The rest time between charge and discharge was set to 0.5 h.

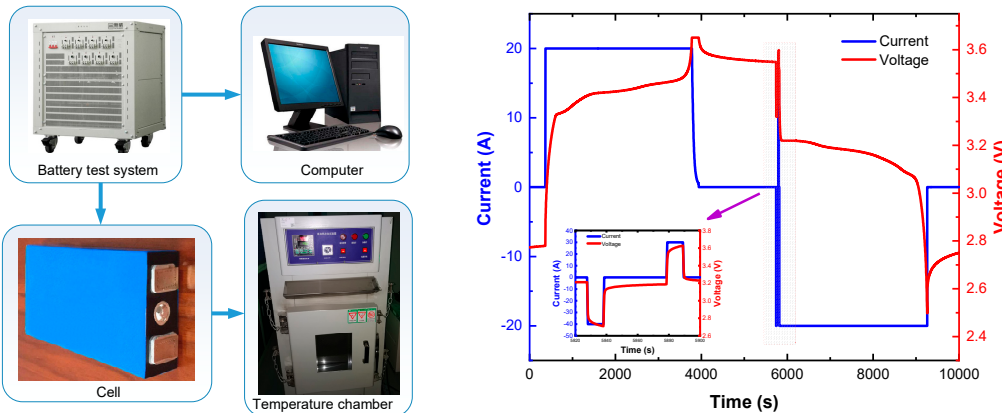


Figure 1. Experiment setup for the aging test.

Table 1. Specification of cells used in the experiment.

Item	
Nominal capacity	20 Ah
Nominal voltage	3.2 V
Charging cut-off voltage	3.65 V
Discharge cut-off voltage	2.5 V
Dimension	133 × 70 × 28 mm ³
Temperature	35 °C
Sampling frequency	1 s

2.2. IC Curve Acquisition and Feature Extraction

Incremental capacity analysis is a widely used technique to obtain information on the electrochemical properties of a cell and unveil degradation mechanisms. IC curves describe the increment of battery capacity within an interval of voltage. The calculation formula is given in Equation (3).

$$IC = \frac{dQ}{dV} = \frac{\Delta Q}{\Delta V} \quad (1)$$

where ΔQ is the increment of capacity in the charge/discharge cycles. ΔV is the corresponding voltage interval.

The IC curve reveals the phase-equilibrium-induced voltage plateau. The peaks of curves are in the range of the voltage plateau. In the voltage plateau region, the capacity increases rapidly with small voltage changes. Due to the limited voltage sampling frequency of charging and discharging equipment, the linear interpolation method was used to obtain the capacity with equal voltage intervals. A large voltage interval may miss some significant information in this region. To obtain complete information on the IC curve as soon as possible, the small voltage internal was set as 1 mV. The peak value of the IC curve and its corresponding voltage platform are shown in Figure 2. The slope of the voltage capacity (V-Q) curve has three obvious changes, which correspond to the three conspicuous peaks of the IC curve. Each peak represents the phase transition point of the materials inside cells, which can characterize the lithiation plateau, transforming into different lithiation stages. The area enclosed by the curve and axis manifests the capacity change in the phase transition. From the picture, it can be observed that the raw IC in the range of the voltage plateau fluctuates greatly. Therefore, it is necessary to smooth the original curves through a filtering algorithm. In this work, the Gaussian filter method was adopted to preprocess

the raw IC curves, which can alleviate the effect of the interference in different cycles on significant IC curve feature extractions.

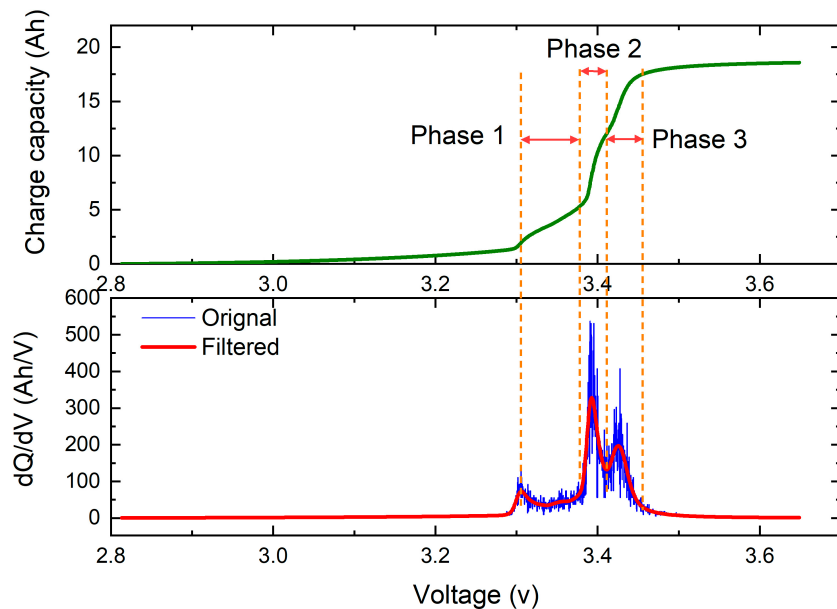


Figure 2. Capacity variation with voltage and IC curve during a charging cycle.

To investigate the relationship between the charge capacity and voltage, partial V-Q curves during 700 cycles are demonstrated in Figure 3. The curves almost overlap in the range from 2.7 V to 3.15 V. In the range of 3.15 V–3.65 V, the difference between curves is relatively large due to capacity degeneration. From this view, as the cycle increases, the position of the voltage plateau is offset to the right. This phenomenon suggests that the peaks of IC curves shift as the battery ages. However, as the cycle progresses, this trend becomes less significant. From the enlarged view, the slope of the voltage plateau becomes slowed down from cycle 1 to cycle 701, especially in phase 3. In other words, the heights of peaks decrease with battery degradation.

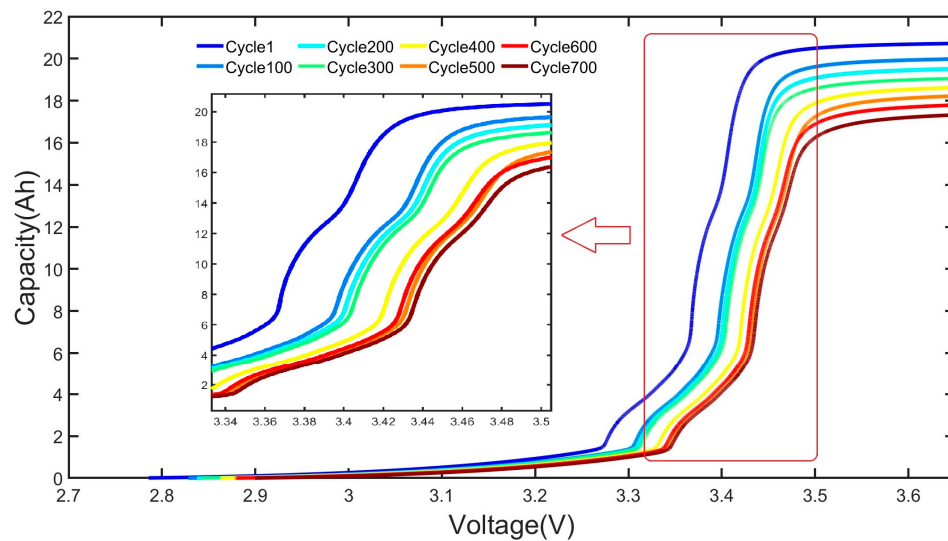


Figure 3. V-Q curves of battery in different aging states during a charge cycle.

To further verify these findings, all the IC curves during 701 cycles are demonstrated in Figure 4. It is evident that the positions of curve peaks shift and the height of the peaks changes, especially the third peak. Moreover, the initial and end voltage values

of the voltage platform are also different. As a battery ages, the peaks may become less pronounced, and the IC curve may flatten overall. This demonstrates that changes in the positions, shapes, and heights of peaks and dips over time can provide information about a battery's state of health. Therefore, we extracted the features of IC curves considering these changes, and the features include the positions of peaks (L_{P1}, L_{P2}, L_{P3}), heights of peaks (H_{P1}, H_{P2}, H_{P3}), width of peaks (W_{P1}, W_{P2}, W_{P3}), positions of dips (L_{d1}, L_{d2}, L_{d3}), and heights of dips (H_{d1}, H_{d2}, H_{d3}), as shown in Figure 5. It was observed that all the peak features were in the voltage range of 3.2 V to 3.5 V. The state of charge of batteries in the voltage range was 20–85%, which is exactly the actual working range of most battery systems such as electric vehicles.

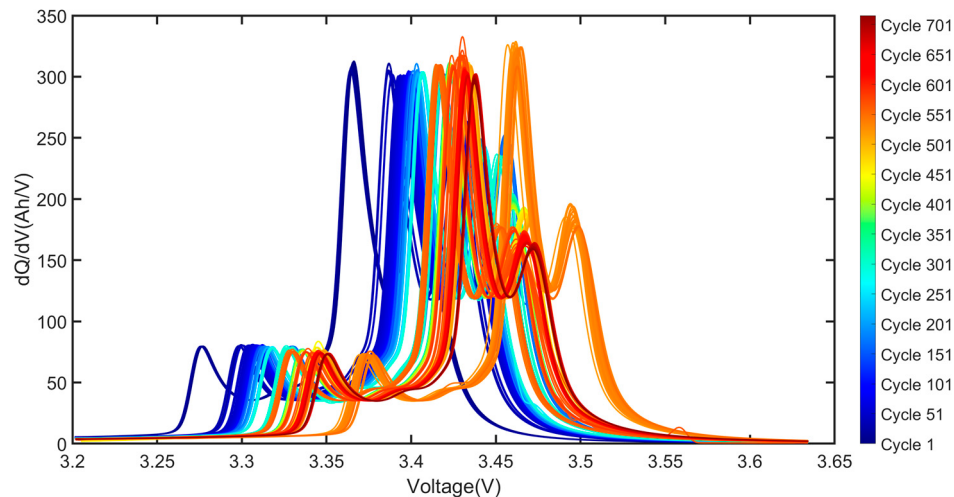


Figure 4. Variations in IC curves during 700 cycles.

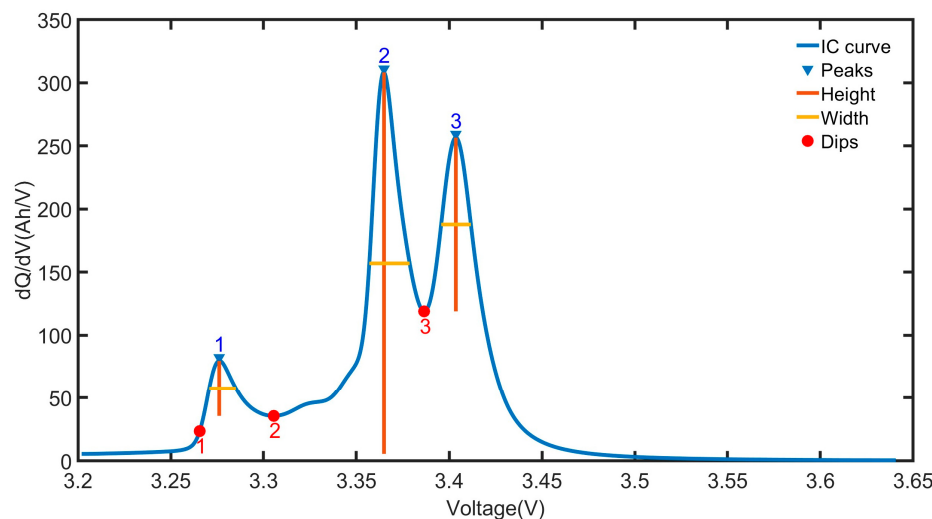


Figure 5. Features extracted from the IC curve.

2.3. Internal Resistance Identification

2.3.1. Model Establishment

Equivalent circuit models are widely used to recognize and estimate the internal parameters of batteries, which are crucial for understanding and managing battery performance. These models provide a simplified representation of the complex electrochemical processes occurring within the battery, making it easier to analyze and control. Commonly used equivalent circuit models of batteries include Rint, Thevenin, 2RC, PNGV, and GNL models. The Rint model is simple, involving only an OCV and a single resistor, which does not capture the dynamic response of the battery to changing loads and conditions, leading

to less accurate predictions of battery performance. The single RC branch in the Thevenin model captures only basic transient behavior, leading to less accurate representations of the battery's dynamic performance, especially under varying load conditions. The PNGV and GNL models are more sophisticated battery models, so the process of identifying and calibrating the parameters is more complex and time-consuming compared to the 2RC model. The 2RC model provides a more accurate representation of a battery's behavior, especially under varying load conditions. By including two RC pairs, this model captures both the short-term and long-term dynamics of the battery, reflecting its real-world performance more closely. Compared to the Thevenin model, the 2RC model can more effectively represent these non-linearities, improving the predictive capability of simulations and control systems. By capturing both fast and slow dynamics, the second-order RC model can provide better insight into the SOH of the battery. This allows for more precise monitoring and diagnostics of parameters like internal resistance and capacitance, which are indicative of aging and degradation. A 2RC equivalent circuit model was used in this work, as shown in Figure 6. R_0 , R_1 , and R_2 represent the ohmic internal resistance and polarization resistance of cells, respectively. The dynamics of 2RC circuits can be given as shown in Equation (2) [31].

$$\begin{aligned} U_{oc}(t) - U_L(t) &= U_{P1}(t) + U_{P2}(t) + i(t)R_0 \\ \dot{U}_1(t) &= \frac{i(t)}{C_1} - \frac{U_1}{C_1 R_1} \\ \dot{U}_2(t) &= \frac{i(t)}{C_2} - \frac{U_2}{C_2 R_1} \end{aligned} \quad (2)$$

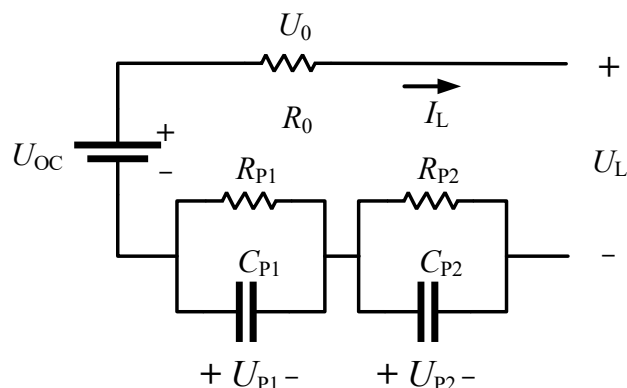


Figure 6. RC equivalent circuit model of batteries.

According to Equation (2), the complex frequency domain dynamics model of the 2RC circuit can be given in

$$U_{oc}(s) - U_L(s) = I(s) \left(R_0 + \frac{R_1}{R_1 C_1 s + 1} + \frac{R_2}{R_2 C_2 s + 1} \right) \quad (3)$$

The transfer function is expressed as

$$G(s) = \frac{U_{oc}(s) - U_L(s)}{I(s)} = \left(R_0 + \frac{R_1}{R_1 C_1 s + 1} + \frac{R_2}{R_2 C_2 s + 1} \right) \quad (4)$$

The z-transform can be used to discretize the above continuous equation by the following equation:

$$s = \frac{2(1 - z^{-1})}{T(1 - z^{-1})} \quad (5)$$

Through a combination of Equations (4) and (5), the discrete transferring function can be expressed as

$$G(z^{-1}) = \frac{a_3 + a_4 z^{-1} + a_5 z^{-2}}{1 - a_1 z^{-1} - a_2 z^{-2}} \quad (6)$$

$$\left\{ \begin{array}{l} a_1 = \frac{8\tau_1\tau_2 - 2T^2}{T^2 + 4\tau_1\tau_2 + 2T\tau_1 + 2T\tau_2} \\ a_2 = \frac{2T\tau_1 + 2T\tau_2 - T^2 - 4\tau_1\tau_2}{T^2 + 4\tau_1\tau_2 + 2T\tau_1 + 2T\tau_2} \\ a_3 = \frac{T^2R_1 + T^2R_2 + 2TR_1\tau_2 + 2TR_2\tau_1}{T^2 + 4\tau_1\tau_2 + 2T\tau_1 + 2T\tau_2} \\ a_4 = \frac{2T^2R_1 + 2T^2R_2}{T^2 + 4\tau_1\tau_2 + 2T\tau_1 + 2T\tau_2} \\ a_5 = \frac{T^2R_1 + T^2R_2 - 2TR_1\tau_2 - 2TR_2\tau_1}{T^2 + 4\tau_1\tau_2 + 2T\tau_1 + 2T\tau_2} \end{array} \right. \quad (7)$$

where T is the sampling interval. a_1, a_2, a_3, a_4 , and a_5 are the coefficients related to the model parameters. $\tau_1 = R_1C_1$, and $\tau_2 = R_2C_2$.

The differential equation of the RC model is given as

$$U(k) = a_1U(k-1) + a_2U(k-2) + a_3I(k) + a_4I(k-1) + a_5I(k-2) \quad (8)$$

The RLS algorithm is extensively employed in battery parameter identification due to its efficiency and accuracy in the real-time estimation of dynamic systems. The RLS algorithm is an adaptive filter algorithm that recursively finds the coefficients that minimize a weighted linear least squares cost function relating to the input signals. It is well suited for systems where parameters change over time, making it ideal for battery modeling. The model can be described by the recursive process of the RLS algorithm as follows:

$$\begin{aligned} U(k) &= \varphi^T(k)\theta(k) \\ \varphi(k) &= [U(k-1), U(k-2), I(k), I(k-1), I(k-2)]^T \\ \theta(k) &= [a_1, a_2, a_3, a_4, a_5]^T \end{aligned} \quad (9)$$

Combining the above equations, the parameters can be expressed as

$$\begin{aligned} R_0 &= [a_3 - a_4 + a_5] / [1 + a_1 - a_2] \\ R_1C_1R_2C_2 &= [T^2(1 + a_1 - a_2)] / [4(1 - a_1 - a_2)] \\ R_1C_1 + R_2C_2 &= [T(1 + a_2)] / [1 - a_1 - a_2] \\ R_0 + R_1 + R_2 &= [a_3 - a_4 + a_5] / [1 - a_1 - a_2] \\ R_0R_1C_2 + R_0R_2C_2 + R_1R_2C_1 + R_1R_2C_2 &= T[a_5 - a_3] / [1 - a_1 - a_2] \end{aligned} \quad (10)$$

The parameters of the equivalent circuit model can be determined by calculating Equation (10).

2.3.2. Identification Results

The Hybrid Pulse Power Characterization (HPPC) test profile was added in each discharge cycle, as demonstrated in Figure 4, and was used to generate data for identifying the parameters of 2RC models. Internal resistance varies with the environmental temperature, the SOC of batteries, and the SOH. To eliminate the interference of temperature and the SOC, testing was carried out in a constant environment temperature, and the HPPC test was conducted in the same SOC state during the discharge phase. The data of HPPC were used to identify the parameters of the 2RC model by the RLS algorithm, as shown in Figure 7. As demonstrated in Figure 7a, the predicted terminal voltage was in good agreement with the experimental one. The error between the predicted and experimental is illustrated in Figure 7b, and the mean absolute error was less than 0.4 mV. This indicates that the identified parameters accurately represented the battery's behavior. The identified parameters of the equivalent model are shown in Figure 7c,d. The average value of the identification parameters during the relaxation phase was taken as the final value for each parameter.

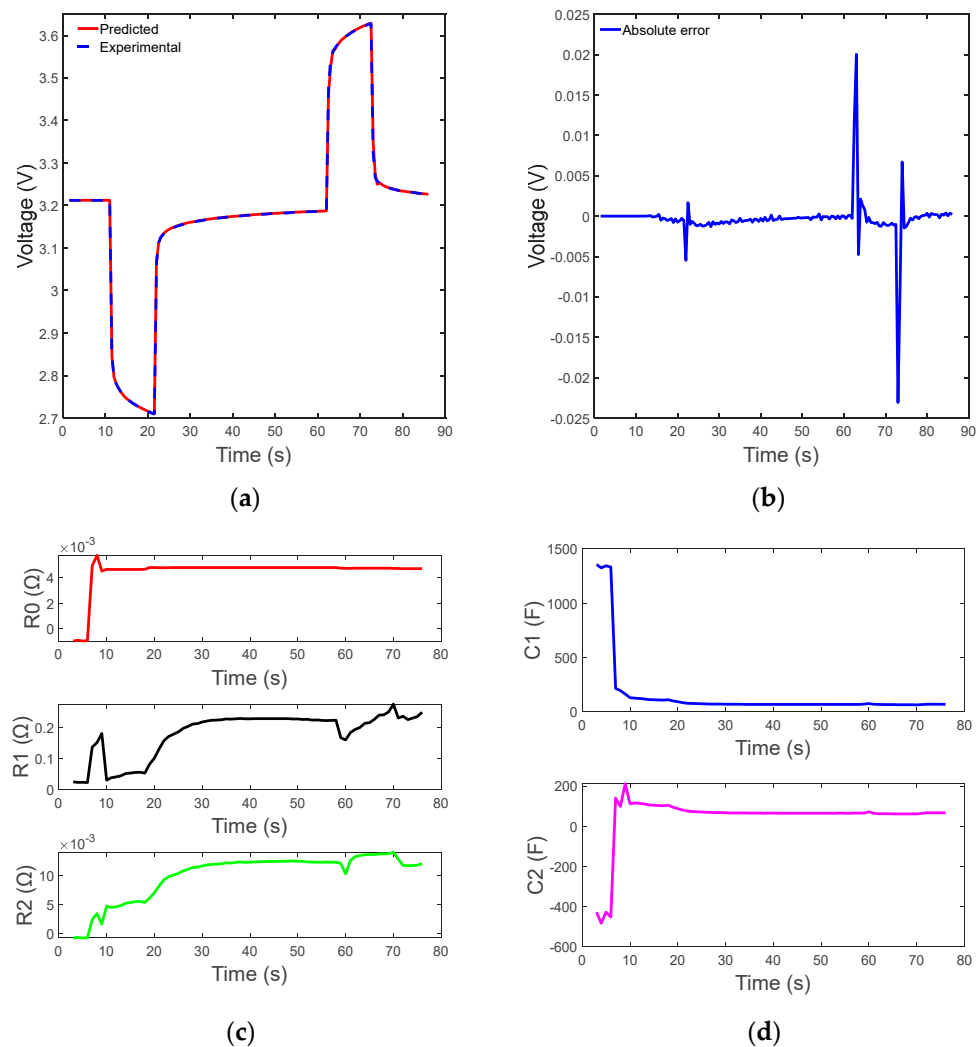


Figure 7. Results of parameter identification for the 2RC equivalent circuit model. (a) the comparison of simulated and experimental voltage; (b) the simulation error; (c) and (d) the identification value of R_0 , R_1 , R_2 , C_1 , C_2 .

3. SOH Estimation Based on LSTM-KAN

3.1. LSTM-KAN Architecture

A Long Short-Term Memory Network is a special type of Recurrent Neural Network (RNN) capable of learning long-term dependencies, which has since been widely adopted for various tasks involving sequential data. The core component of an LSTM network is the memory cell, which can maintain its state over time. This allows the network to remember important information for long periods. LSTMs have three types of gates that regulate the flow of information, including forget gate, input gate, and output gate. The forget gate decides which parts of the cell state to forget. It takes the previous hidden state (h_{t-1}) and the current input (x_t) and passes them through a sigmoid function, as follows:

$$f_t = \sigma(W_f \cdot [h_{t-1}, x_t] + b_f) \quad (11)$$

The input gate decides which new information to store in the cell state. It has two parts: the input gate layer and candidate values. The former determines which values to update, and the latter creates new candidate values to be added to the state. The formulas of the input gate layer and candidate values can be described as follows:

$$i_t = \sigma(W_i \cdot [h_{t-1}, x_t] + b_i) \quad (12)$$

$$\tilde{C}_n = \tanh(W_c \cdot [h_{t-1}, x_t] + b_c) \quad (13)$$

The new cell state is a combination of the old state and the new candidate values.

$$C_t = f_t \cdot C_{t-1} + i_t \cdot \tilde{C}_t \quad (14)$$

The output gate determines the next hidden state, which is a filtered version of the cell state.

$$O_t = \sigma(W_o \cdot [h_{t-1}, x_t] + b_o) \quad (15)$$

The hidden state output of the network node is described and calculated by this equation, as follows:

$$h_t = O_t \tanh(C_t) \quad (16)$$

Kolmogorov–Arnold Networks (KANs) are a novel network architecture proposed by the MIT team in May 2024, which were inspired by the Kolmogorov–Arnold representation theorem [15], as shown in Figure 8. This theorem states that any multivariable continuous function can be decomposed into a finite sum of continuous functions of one variable and an additional continuous function. Leveraging this theoretical foundation, Kolmogorov–Arnold Networks aim to simplify the representation of complex functions and improve the efficiency and interpretability of neural networks.

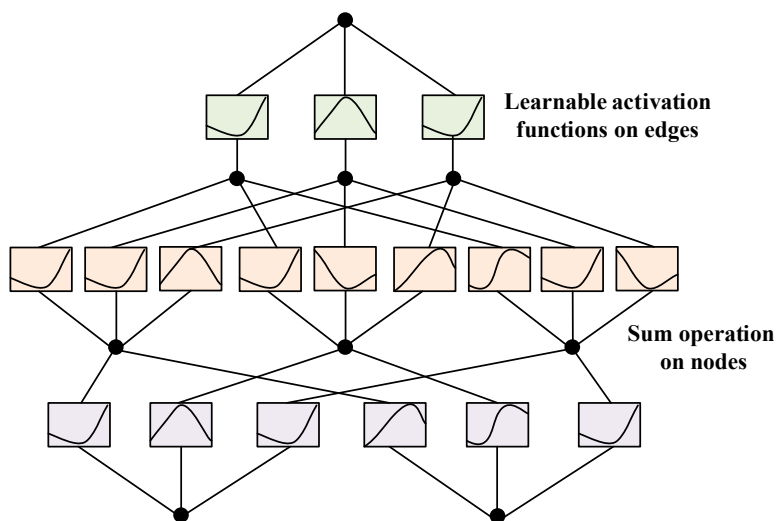


Figure 8. Kolmogorov–Arnold Network architecture.

The architecture of KANs typically involves a decomposition of the input space into individual dimensions, followed by processing through one-dimensional functions before combining the results. The theorem can be expressed as follows:

$$f(x_1, \dots, x_n) = \sum_{q=1}^{2n+1} \Phi_q \left(\sum_{p=1}^n \varphi_{q,p}(x_p) \right) \quad (17)$$

where $\varphi_{q,p}$ are univariate functions that map each input variable x_p , and Φ_q are continuous functions. This enables a KAN to model complex interactions in high-dimensional data by breaking them down into compositions of simpler univariate functions.

A KAN layer with n_{in} -dimensional inputs and n_{out} -dimensional outputs can be defined as a matrix of 1D functions.

$$\Phi = \{\varphi_{q,p}\}, p = 1, 2, \dots, n_{\text{in}}, q = 1, 2, \dots, n_{\text{out}} \quad (18)$$

where the $\varphi_{q,p}$ is parametrized functions with 1 trainable parameter.

A deeper KAN is composed of multiple KAN layers with a strong ability to model more complex functions. The architecture of a deeper KAN can be expressed as follows:

$$KAN(x) = (\Phi_{L-1} \circ \Phi_{L-2} \circ \dots \circ \Phi_0)(x) \quad (19)$$

LSTM-KAN combines the strengths of LSTM networks with the theoretical insights of Kolmogorov–Arnold Networks to model complex, time-dependent relationships in high-dimensional data. This hybrid approach leverages an LSTM’s ability to handle sequential data and a KAN’s capacity for simplifying multivariate functions into compositions of univariate functions. The hybrid network is implemented by integrating a KAN directly into the hidden layer of an LSTM network. This can be especially useful for applications requiring both temporal sequence analysis and complex feature interactions.

3.2. SOH Estimation Model Framework

In the above section, the features of IC curves and the parameters of internal resistance were obtained. Next, the extracted features and internal resistance were taken as input parameters, and the output was the SOH. From Figure 4, it is observed that the IC curves did not all shift to the right as the cycle increased; rather, the curve offset presented a time series characteristic. Here, the LSTM network was used to process the IC curve features and internal resistance parameters and capture the temporal dependencies. In the hidden layer before output, the KAN layer was used to replace the standard fully connected layers in the LSTM. The structure of the proposed SOH estimation model based on LSTM-KAN is shown in Figure 9. This framework provides a robust approach to estimate the battery SOH using LSTM-KAN and features derived from IC curves, leveraging the strengths of the LSTM in handling sequential data and the KAN in decomposing complex multivariate functions to achieve accurate and reliable SOH predictions. The input parameter matrix consists of 18 parameters, including 15 IC features, and 5 parameters of 2RC equivalent circuit models.

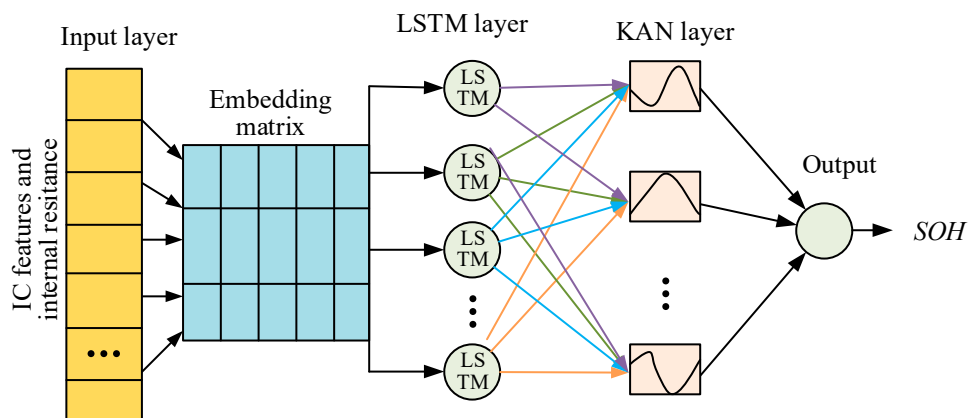


Figure 9. Structure of LSTM-KAN used for SOH estimation.

3.3. Evaluation of the Error of the SOH

Evaluating the error of SOH estimation models is critical in order to ensure their accuracy and reliability. Three error metrics are utilized to evaluate the performance of different estimation models.

Mean Absolute Error (MAE)

$$MAE = \frac{1}{n} \sum_{i=1}^n |y_i - \hat{y}_i| \quad (20)$$

Mean Absolute Error (MAPE)

$$\text{MAPE} = \frac{1}{n} \sum_{i=1}^n \left| \frac{y_i - \hat{y}_i}{y_i} \right| * 100\% \quad (21)$$

Mean Absolute Error (RMSE)

$$\text{RMSE} = \sqrt{\frac{1}{n} \sum_{i=1}^n (y_i - \hat{y}_i)^2} \quad (22)$$

where y_i and \hat{y}_i are the real value and predicted value at test cycle I , and n is the total of the test cycles.

4. Results of SOH Estimation

4.1. The SOH Estimated by the LSTM-KAN Model

The data used in this experiment come from the accelerated aging test, and eight batteries with different initial SOHs were selected as the samples. Four fresh cells and four cells with the same specifications were selected for the aging tests. The initial SOH and aging cycles experienced are shown in Table 2. Selecting batteries with different SOH values not only enriches the sample types in the training data but can also be used to verify the generalization ability of the estimation model under different SOH conditions.

Table 2. SOH initial values and the experienced cycles of battery samples.

	Bat. #1	Bat. #2	Bat. #3	Bat. #4	Bat. #5	Bat. #6	Bat. #7	Bat. #8
SOH	100%	100%	100%	100%	90.3%	87.9%	88.09%	96.18%
Cycles	500	1070	930	380	550	375	320	590

The training dataset is composed of the IC features and parameters of the equivalent circuit of six batteries (Bat. #1, #2, #3, #6, #7, and #8). The data of Bat. #4 and Bat. #8 are used as the test and validation dataset, respectively. The SOH of Bat. #4 was estimated using the three most commonly used machine learning methods and the hybrid models based on the KAN, as shown in Figure 10. The actual SOH shows a steady decline over the cycle range, from 0 to 600. The SOH value predicted by the five models follows the general trend in the actual SOH but with different degrees of fluctuation. From the picture, the SOH predicted by the BP model has significant deviation from the actual value. The values estimated by the LSTM-KAN and TCN-KAN models are better matched with the actual SOH. The results indicate that while the conventional models can capture the overall degradation trend, they show some noise or variability in their predictions. The SOH predicted by hybrid models closely follows the actual value with less fluctuation.

To ensure the trained model's robustness and generalization ability, a validation dataset was used to evaluate its performance. The data for Bat. #5 were used as the validation dataset. The results of the validation are illustrated in Figure 11, which demonstrates that the trained models also have good performance on the validation dataset. The values predicted by the five models show a similar trend to the actual SOH but with a noticeable offset from the actual SOH in the BP and TCN models. From the enlarged view, it can be observed that the SOH predicted by the LSTM-KAN model is closer to the actual value. Similar to the results of the test data, the prediction error of the BP model is the largest in the validation dataset.

The results of the test and validation data confirm the superior performance and generalization ability of the hybrid model compared to the standalone network. The consistency of the hybrid model's performance across both the training and validation datasets suggests that it effectively captures the underlying patterns of battery degradation. This demonstrates that the hybrid model not only performs well on the training data but

also maintains high accuracy and stability when applied to new data. The error metrics of the five models on the test and validation dataset are shown in Table 3. It demonstrates that the prediction errors of the BP model are the largest among the five models. All the errors of the hybrid model are smaller than those of the original model. In the test dataset, the LSTM-KAN model has the fewest errors, and the MAE, MAPE, and RMSE are 0.412%, 0.462%, and 0.570%, respectively. In the validation dataset, the MAE of the LSTM and LSTM-KAN are 0.438% and 0.256%, which is in good agreement with the results of the test data. The SOH estimation performance of the LSTM-KAN and TCN-KAN models is comparable. The above results demonstrate that combining the KAN can effectively improve the estimation performance of conventional machine learning models, and the LSTM-KAN model has the best performance in SOH estimation, with a comprehensive comparison of testing and validation data results. Therefore, the LSTM-KAN model was used to further investigate the model performance under different input parameters. The training time of each model is shown in Figure 12. In Refs. [11,12], the SOH estimation models are established based on similar methods, but the estimation error (MAE: 1.16%, 1.957%) of the model in the literature is far larger than that proposed in this work (MAE: 0.412%).

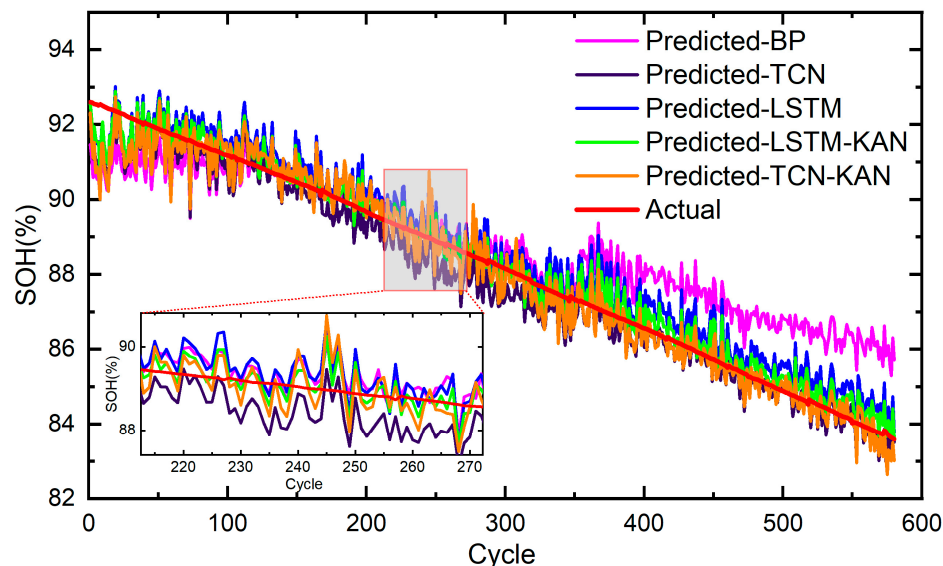


Figure 10. Predicted SOH of Bat. #4 for the test dataset.

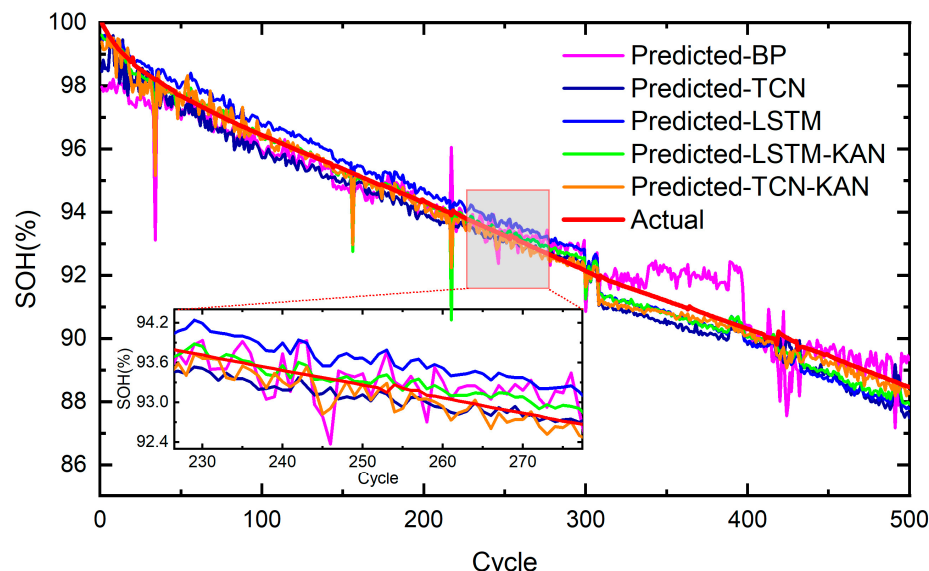
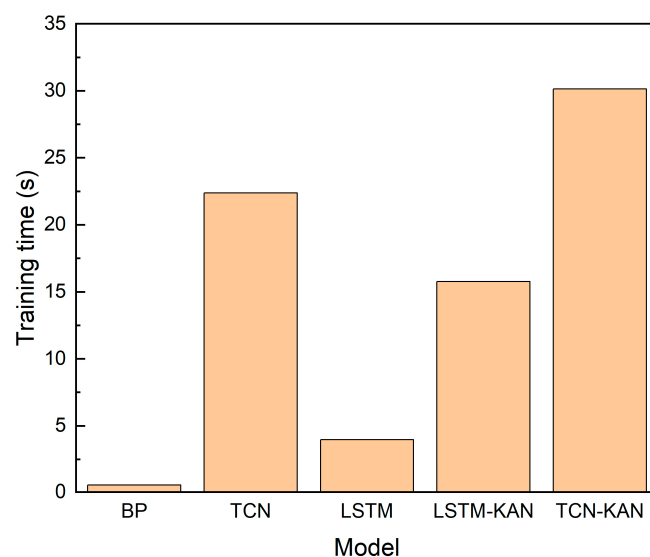


Figure 11. SOH of Bat. #5 predicted by the trained model.

Table 3. SOH estimation errors of two models in different datasets.

	MAE	MAPE	RMSE
Test-BP	0.811%	0.921%	1.028%
Test-TCN	0.472%	0.528%	0.607%
Test-LSTM	0.519%	0.585%	0.641%
Test-LSTM-KAN	0.412%	0.462%	0.570%
Test-TCN-KAN	0.426%	0.476%	0.572%
Validation-BP	0.531%	0.569%	0.727%
Validation-TCN	0.461%	0.495%	0.547%
Validation-LSTM	0.438%	0.472%	0.490%
Validation-LSTM-KAN	0.256%	0.278%	0.378%
Validation-TCN-KAN	0.251%	0.268%	0.365%

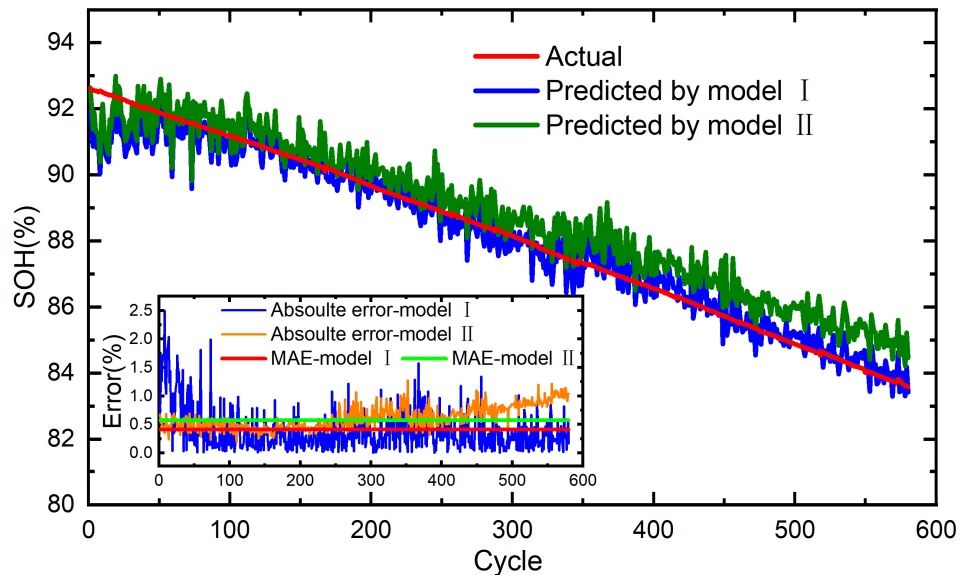
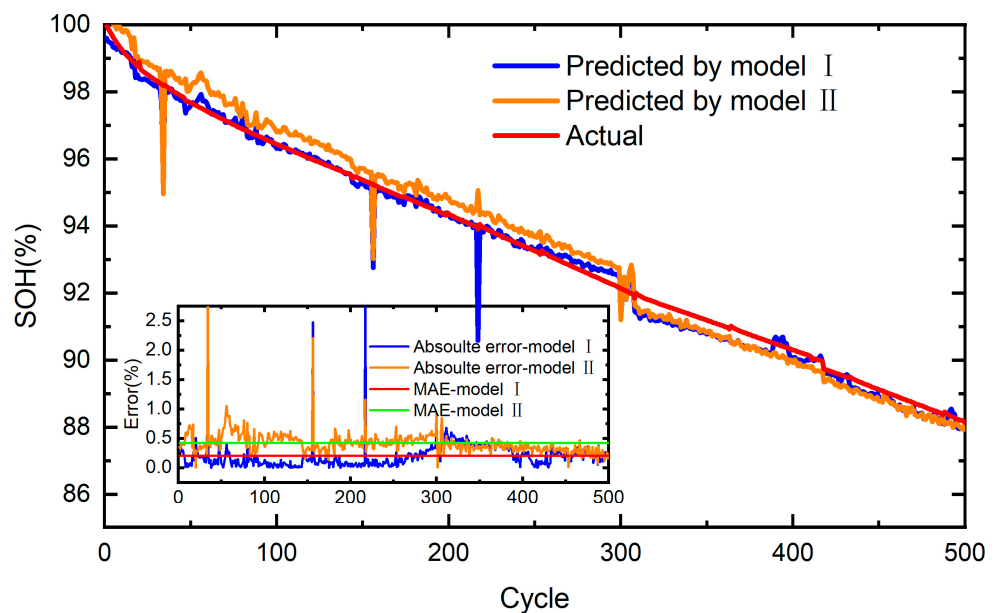
**Figure 12.** Training time of each model.

4.2. The SOH Estimated by the LSTM-KAN Model with Different Input Variables

To investigate the improvement of the model after integrating internal resistance parameters into the input variables, the training data were divided into two groups: group I and group II. The input variables in model I include 15 features extracted from IC curves and internal resistance parameters, and those in model II only contain 15 features extracted from IC curves, as demonstrated in Table 4. The corresponding SOH estimation models, model I and model II, were trained using datasets from group I and group II, respectively. Figure 13 illustrates the SOH of Bat. #5 predicted by two models. The results show that the predicted SOH is closely aligned with the actual value. Model II shows greater variability and deviations from the actual SOH compared to model I. The performance of the two models on the validation samples is demonstrated in Figure 14. Similarly, model I demonstrates better prediction performance than that of model II. From the subplots, model I has a lower MAE in the test and validation dataset. This indicates that the integration of internal resistance parameters into the input parameters can improve the model's performance.

Table 4. Input and output variables of model I and model II.

	Input	Output
Model I	$L_{P1}, L_{P2}, L_{P3}, H_{P1}, H_{P2}, H_{P3}, W_{P1}, W_{P2}, W_{P3}, L_{d1}, L_{d2}, L_{d3}, H_{d1}, H_{d2}, H_{d3}, R_0, R_1, R_2, C_1, C_2$	SOH
Model II	$L_{P1}, L_{P2}, L_{P3}, H_{P1}, H_{P2}, H_{P3}, W_{P1}, W_{P2}, W_{P3}, L_{d1}, L_{d2}, L_{d3}, H_{d1}, H_{d2}, H_{d3}$	SOH

**Figure 13.** SOH of Bat. #4 predicted by different models.**Figure 14.** Results of Bat. #5 predicted by the trained model.

5. Conclusions

In this paper, we presented an innovative approach for estimating the SOH of Li-ion batteries by integrating incremental capacity analysis and internal resistance identification, using a hybrid model of traditional machine learning models and a KAN. The results demonstrate that the proposed hybrid model has good performance for SOH estimation in the test and validation dataset. The hybrid model integrated with the KAN effectively captured the complex relationships among the input features, leveraging its architecture

to improve estimation performance. The accuracy of the hybrid models is higher than that of conventional models, which illustrates that hybrid models combined with KANs can enhance the accuracy and reliability of SOH predictions. The comparison of models with different inputs showed that including internal resistance as input parameters can enhance the accuracy of the model compared to using only IC features. All input features of the model were extracted from the charge data within the SOC range of 20% to 80%. The proposed model does not require full charge and discharge data. This framework shows promising application prospects in battery management systems of electric vehicles, which can facilitate more accurate monitoring and fast detection of battery SOHs.

Author Contributions: Writing—original draft, J.P.; funding acquisition, X.Z.; supervision, J.M.; investigation, D.M.; Methodology, S.J.; Formal analysis, K.Z.; visualization, C.G. and W.D. All authors have read and agreed to the published version of the manuscript.

Funding: This work was partially supported by the Shaanxi Postdoctoral Science Foundation (2023BSHEDZZ222), Fundamental Research Funds for the Central Universities, CHD (300102223103), National Natural Science Foundation of China (52172362, 52372375), Scientific and technological achievements transformation plan project of Shaanxi Province (2024CG-CGZH-19), and Key research and development plan project of Shaanxi Province (2024GX-YBXM-260).

Data Availability Statement: The original contributions presented in the study are included in the article, further inquiries can be directed to the corresponding author.

Conflicts of Interest: The authors declare no conflicts of interest.

References

- Peng, J.; Zhou, X.; Jia, S.; Jin, Y.; Xu, S.; Chen, J. High precision strain monitoring for lithium ion batteries based on fiber Bragg grating sensors. *J. Power Sources* **2019**, *433*, 226692. [[CrossRef](#)]
- Lu, L.; Han, X.; Li, J.; Hua, J.; Ouyang, M. A review on the key issues for lithium-ion battery management in electric vehicles. *J. Power Sources* **2013**, *226*, 272–288. [[CrossRef](#)]
- Berecibar, M.; Gandiaga, I.; Villarreal, I.; Omar, N.; Van Mierlo, J.; Van den Bossche, P. Critical review of state of health estimation methods of Li-ion batteries for real applications. *Renew. Sustain. Energy. Rev.* **2016**, *56*, 572–587. [[CrossRef](#)]
- Ng, K.S.; Moo, C.-S.; Chen, Y.-P.; Hsieh, Y.-C. Enhanced coulomb counting method for estimating state-of-charge and state-of-health of lithium-ion batteries. *Appl. Energy* **2009**, *86*, 1506–1511. [[CrossRef](#)]
- Lu, J.; Xiong, R.; Tian, J.; Wang, C.; Sun, F. Deep learning to estimate lithium-ion battery state of health without additional degradation experiments. *Nat. Commun.* **2023**, *14*, 2760. [[CrossRef](#)]
- Song, S.; Fei, C.; Xia, H. Lithium-Ion Battery SOH Estimation Based on XGBoost Algorithm with Accuracy Correction. *Energies* **2020**, *13*, 812. [[CrossRef](#)]
- Chen, L.; Lü, Z.; Lin, W.; Li, J.; Pan, H. A new state-of-health estimation method for lithium-ion batteries through the intrinsic relationship between ohmic internal resistance and capacity. *Measurement* **2018**, *116*, 586–595. [[CrossRef](#)]
- Li, X.; Wang, Z.; Zhang, L.; Zou, C.; Dorrell, D.D. State-of-health estimation for Li-ion batteries by combining the incremental capacity analysis method with grey relational analysis. *J. Power Sources* **2019**, *410–411*, 106–114. [[CrossRef](#)]
- Weng, C.; Cui, Y.; Sun, J.; Peng, H. On-board state of health monitoring of lithium-ion batteries using incremental capacity analysis with support vector regression. *J. Power Sources* **2013**, *235*, 36–44. [[CrossRef](#)]
- Zhang, M.; Chen, W.; Yin, J.; Feng, T. Lithium Battery Health Factor Extraction Based on Improved Douglas–Peucker Algorithm and SOH Prediction Based on XGboost. *Energies* **2022**, *15*, 5981. [[CrossRef](#)]
- Wen, J.; Chen, X.; Li, X.; Li, Y. SOH prediction of lithium battery based on IC curve feature and BP neural network. *Energy* **2022**, *261*, 125234. [[CrossRef](#)]
- Fan, Z.; Zi-xuan, X.; Ming-hu, W. State of health estimation for Li-ion battery using characteristic voltage intervals and genetic algorithm optimized back propagation neural network. *J. Energy Storage* **2023**, *57*, 106277. [[CrossRef](#)]
- Li, W.; Sengupta, N.; Dechent, P.; Howey, D.; Annaswamy, A.; Sauer, D.U. Online capacity estimation of lithium-ion batteries with deep long short-term memory networks. *J. Power Sources* **2021**, *482*, 228863. [[CrossRef](#)]
- Gong, Y.; Zhang, X.; Gao, D.; Li, H.; Yan, L.; Peng, J.; Huang, Z. State-of-health estimation of lithium-ion batteries based on improved long short-term memory algorithm. *J. Energy Storage* **2022**, *53*, 105046. [[CrossRef](#)]
- Liu, Z.; Wang, Y.; Vaidya, S.; Ruehle, F.; Halverson, J.; Soljačić, M.; Hou, T.Y.; Tegmark, M. Kan: Kolmogorov-arnold networks. *arXiv* **2024**, arXiv:2404.19756.
- Vaca-Rubio, C.J.; Blanco, L.; Pereira, R.; Caus, M. Kolmogorov-arnold networks (kans) for time series analysis. *arXiv* **2024**, arXiv:2405.08790.

17. Pastor-Fernández, C.; Uddin, K.; Chouchelamane, G.H.; Widanage, W.D.; Marco, J. A Comparison between Electrochemical Impedance Spectroscopy and Incremental Capacity-Differential Voltage as Li-ion Diagnostic Techniques to Identify and Quantify the Effects of Degradation Modes within Battery Management Systems. *J. Power Sources* **2017**, *360*, 301–318. [[CrossRef](#)]
18. Zheng, L.; Zhu, J.; Lu, D.D.-C.; Wang, G.; He, T. Incremental capacity analysis and differential voltage analysis based state of charge and capacity estimation for lithium-ion batteries. *Energy* **2018**, *150*, 759–769. [[CrossRef](#)]
19. Jiang, B.; Dai, H.; Wei, X. Incremental capacity analysis based adaptive capacity estimation for lithium-ion battery considering charging condition. *Appl. Energy* **2020**, *269*, 115074. [[CrossRef](#)]
20. Li, Y.; Abdel-Monem, M.; Gopalakrishnan, R.; Berecibar, M.; Nanini-Maury, E.; Omar, N.; van den Bossche, P.; Van Mierlo, J. A quick on-line state of health estimation method for Li-ion battery with incremental capacity curves processed by Gaussian filter. *J. Power Sources* **2018**, *373*, 40–53. [[CrossRef](#)]
21. Li, X.; Yuan, C.; Wang, Z. State of health estimation for Li-ion battery via partial incremental capacity analysis based on support vector regression. *Energy* **2020**, *203*, 117852. [[CrossRef](#)]
22. Beltran, H.; Sansano, E.; Pecht, M. Machine learning techniques suitability to estimate the retained capacity in lithium-ion batteries from partial charge/discharge curves. *J. Energy Storage* **2023**, *59*, 106346. [[CrossRef](#)]
23. Raccichini, R.; Amores, M.; Hinds, G. Critical Review of the Use of Reference Electrodes in Li-Ion Batteries: A Diagnostic Perspective. *Batteries* **2019**, *5*, 12. [[CrossRef](#)]
24. Barai, A.; Uddin, K.; Widanage, W.D.; McGordon, A.; Jennings, P. A study of the influence of measurement timescale on internal resistance characterisation methodologies for lithium-ion cells. *Sci. Rep.* **2018**, *8*, 21. [[CrossRef](#)] [[PubMed](#)]
25. Meddings, N.; Heinrich, M.; Overney, F.; Lee, J.-S.; Ruiz, V.; Napolitano, E.; Seitz, S.; Hinds, G.; Raccichini, R.; Gaberšček, M.; et al. Application of electrochemical impedance spectroscopy to commercial Li-ion cells: A review. *J. Power Sources* **2020**, *480*, 228742. [[CrossRef](#)]
26. Tan, X.; Tan, Y.; Zhan, D.; Yu, Z.; Fan, Y.; Qiu, J.; Li, J. Real-Time State-of-Health Estimation of Lithium-Ion Batteries Based on the Equivalent Internal Resistance. *IEEE Access* **2020**, *8*, 56811–56822. [[CrossRef](#)]
27. Galeotti, M.; Cinà, L.; Giannanco, C.; Cordiner, S.; Di Carlo, A. Performance analysis and SOH (state of health) evaluation of lithium polymer batteries through electrochemical impedance spectroscopy. *Energy* **2015**, *89*, 678–686. [[CrossRef](#)]
28. Grandjean, T.; Groenewald, J.; McGordon, A.; Widanage, W.; Marco, J. Accelerated Internal Resistance Measurements of Lithium-Ion Cells to Support Future End-of-Life Strategies for Electric Vehicles. *Batteries* **2018**, *4*, 49. [[CrossRef](#)]
29. Mei, W.; Jiang, L.; Liang, C.; Sun, J.; Wang, Q. Understanding of Li-plating on graphite electrode: Detection, quantification and mechanism revelation. *Energy Storage Mater.* **2021**, *41*, 209–221. [[CrossRef](#)]
30. Chahbaz, A.; Meishner, F.; Li, W.; Ünlübayir, C.; Uwe Sauer, D. Non-invasive identification of calendar and cyclic ageing mechanisms for lithium-titanate-oxide batteries. *Energy Storage Mater.* **2021**, *42*, 794–805. [[CrossRef](#)]
31. Ren, B.; Xie, C.; Sun, X.; Zhang, Q.; Yan, D. Parameter identification of a lithium-ion battery based on the improved recursive least square algorithm. *IET Power Electron.* **2020**, *13*, 2531–2537. [[CrossRef](#)]

Disclaimer/Publisher's Note: The statements, opinions and data contained in all publications are solely those of the individual author(s) and contributor(s) and not of MDPI and/or the editor(s). MDPI and/or the editor(s) disclaim responsibility for any injury to people or property resulting from any ideas, methods, instructions or products referred to in the content.